The Annual Range of Southern Hemisphere SST: Comparison with Surface Heating and Possible Reasons for the High-Latitude Falloff*

A. M. CHIODI AND D. E. HARRISON

Joint Institute for the Study of the Atmosphere and the Ocean, University of Washington, and NOAA/Pacific Marine Environmental Laboratory, Seattle, Washington

(Manuscript received 27 March 2009, in final form 12 November 2009)

ABSTRACT

Globally, the seasonal cycle is the largest single component of observed sea surface temperature (SST) variability, yet it is still not fully understood. Herein, the degree to which the structure of the seasonal cycle of Southern Hemisphere SST can be explained by the present understanding of surface fluxes and upper-ocean physics is examined. It has long been known that the annual range of Southern Hemisphere SST is largest in the midlatitudes, despite the fact that the annual range of net surface heat flux peaks well poleward of the SST peak. The reasons for this discrepancy (''falloff of the annual range of SST'') are determined here through analysis of net surface heat flux estimates, observed SST, and mixed layer depth data, and results from experiments using two different one-dimensional ocean models. Results show that (i) the classical explanations for the structure of the annual range of SST in the Southern Hemisphere are incomplete, (ii) current estimates of surface heat flux and mixed layer depth can be used to accurately reproduce the observed annual range of SST, and (iii) the prognostic mixed layer models used here often fail to adequately reproduce the seasonal cycle at higher latitudes, despite performing remarkably well in other regions. This suggests that more work is necessary to understand the changes of upper-ocean dynamics that occur with latitude.

1. Introduction

It is commonly understood that the seasons as we know them are fundamentally caused by solar radiation variability, but a striking difference exists between the structures of surface heat flux forcing and SST. This difference is perhaps seen most clearly in the Southern Hemisphere, where the zonally averaged annual range of SST peaks in the midlatitudes at about 35°S, but the range of the net surface heat flux peaks poleward of 60°S.

The reason for this discrepancy has received varied treatment in classic oceanography texts, but has not been adequately resolved. For example, the Southern Hemisphere case is not discussed by Sverdrup et al. (1942) because the limited number of surface heat flux measurements available at the time [presented by Kimball (1928); only radiative fluxes were considered in this case because of data availability] did not show a significant discrepancy between the shapes of the seasonal ranges of Southern Hemisphere surface heat flux and SST. Defant (1961), however, later provided the following heuristic explanation for the falloff of seasonal range of SST at high latitude (speaking of both the Northern and Southern and Hemispheres):

> With increasing latitude the incoming radiation becomes less effective and the autumn and winter convection, which is able to penetrate down to greater depths here, still further reduces the annual amplitude of the temperature variation until it reaches a minimum in the polar regions (p. 112).

However, a more detailed analysis of this issue is not to be found in this text, perhaps because of the scarcity of surface heat flux information and the lack of contemporary ocean modeling capabilities. Nonetheless, we have found little discussion of this issue in contemporary oceanography texts and literature. For example, Pickard

* Joint Institute for the Study of the Atmosphere and Ocean Contribution Number 1746 and National Oceanic and Atmospheric Pacific Marine Environmental Laboratory Publication Number 3304.

Corresponding author address: A. M. Chiodi, Box 357941, 7600 Sand Point Way NE, NOAA/Pacific Marine Environmental Laboratory, Seattle, WA 98115.
E-mail: andy.chiodi@noaa.gov

DOI: 10.1175/2009JCLI3154.1

© 2010 American Meteorological Society

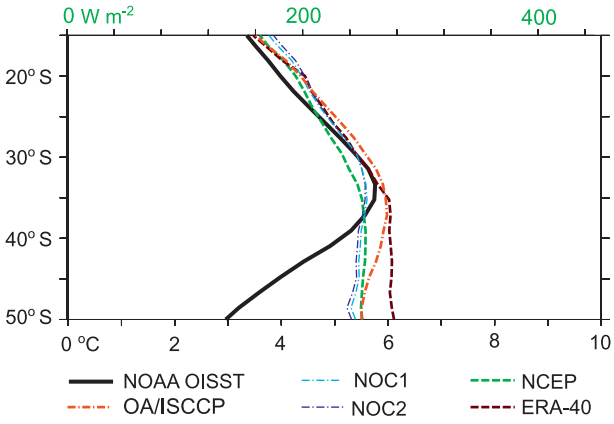

FIG. 1. The annual range of SST from the monthly averaged NOAA OISST climatology (zonal averages shown by solid black curve). Also shown are the annual ranges of net surface heat fluxes from monthly averaged climatologies determined from the NCEP–NCAR reanalysis (green-dashed curve), ERA-40 (brown-dashed curve), the NOC1 (light blue dot–dashed curve) and NOC2 climatologies (dark blue dot–dashed curve), and the OAFlux/ISCCP dataset (orange dot–dashed curve).

and Emery (1990) note only that sea ice, where present, will act as a buffer against large seasonal changes in SST, a process not thought to be important to the basically ice-free regions considered here.

The analysis and experiments presented here examine how well our present understanding of ocean mixed layer physics and contemporary estimates of surface fluxes are able to account for the observed seasonal behavior of SST. The effects of heat flux convergence resulting from the geostrophic ocean currents estimated by contemporary ocean assimilation models are also considered. We focus on latitudes that are broadly centered around 35°S, where the maximum annual range of Southern Hemisphere SST occurs in a zonally averaged sense. Thus, the regions that are considered include one from about 20° to 35°S, in which the annual range of SST increases with latitude in a manner similar to the surface heat fluxes, and a region from about 35° to 50°S in which it does not (see Fig. 1). Polar and tropical regions are not considered here because the tropics and ice-covered regions pose different situations than those mainly considered here.

There are also differences between the structure of the annual ranges of surface heat flux and SST in the Northern Hemisphere, but the character of this relationship is somewhat different in this case. In the Northern Hemisphere, wintertime outbreaks of cold, dry air from the continents help to significantly increase the annual range of SST along the eastern coasts of Asia and North America (Sverdrup et al. 1942). This process does not occur to the same extent in the Southern Hemisphere. Because of this and the relatively smaller sizes of the Northern Hemisphere ocean basins, accurately reproducing the general structure of the seasonal cycle of SST in the Northern Hemisphere requires substantial modeling of regions where heat budgets are influenced by strong western boundary currents [see Dong and Kelly (2004) for a discussion of the upper-ocean heat budget in these regions]. This also poses a somewhat different situation than that mainly considered here. Despite containing some regions, such as the Brazil–Falkland confluence area and the Agulhas return current region, where ocean heat flux convergence may be of primary importance, the upper-ocean heat budget in the Southern Hemisphere has been found to be largely dominated by the temperature tendency and surface heating terms (see references in section 2, below).

Southern Hemisphere SST plays an important role in moderating the overall surface temperature of the Southern Hemisphere. The processes responsible for the falloff of the seasonal cycle of SST in the regions considered here are also likely to be important in polar or near-polar regions, where ocean temperatures and currents near the ice edge have been shown to play an important role in sea ice budgets (e.g., Bitz et al. 2005). Thus, in the interest of increased general knowledge of climate, it is necessary to form a better understanding of the processes that control the observed relationship between the annual range of SST and surface heat flux forcing. Though focus here is on the Southern Hemisphere, we expect that results may also inform our understanding of Northern Hemisphere processes that may otherwise be somewhat masked by interactions between the larger Northern Hemisphere landmasses and western boundary currents.

2. Background

Cherniawsky and Oberhuber (1996) have previously used an ocean general circulation model to predict the global seasonal cycle of SST. Their model underestimated the annual range of SST by 26% averaged over all regions between 60°–10°S and 10°–60°N. The authors ascribed this discrepancy to the atmospheric coupling scheme used in their model. A different approach is used in the model experiments discussed here, in that the surface fluxes are fully determined prior to integration of the ocean model.

Kara et al. (2003) also discuss seasonal SST variability predicted by a multilayer global ocean model with an embedded mixed layer model. This model was found to reproduce the seasonal cycle of SST reasonably well when the surface fluxes were specified using climatological atmospheric conditions and all nonmixed layer ocean temperatures were relaxed to climatological values. Such

methods create an indirect restoring flux, which can significantly affect model results and obscure imperfections in the model physics. In the present case, surface fluxes are specified prior to integration, so that imperfections in the fluxes and the model can be more easily identified, and the fidelity of our present knowledge of mixed layer dynamics can be assessed.

Recently, Dong et al. (2007) published an assessment of the Southern Ocean mixed layer heat budget, showing reasonable closure in a spatially averaged sense (average imbalance on the order of 3×10^{-7}°C s^{-1}). Averaged over ocean regions between 40° and 60°S, the authors report that the temperature tendency is mainly balanced by the surface heating term, which was found to be sensitive to mixed layer depth.

Previous regional studies of the ocean mixed layer heat budget have shown the details of the upper-ocean heat balance to depend on location. These are too numerous to summarize thoroughly here, but of particular relevance is the upper-ocean heat balance conducted at Ocean Weather Station (OWS) Papa, where Davis et al. (1981) concluded that heat content changes at OWS Papa were mainly balanced by surface heating. In a later study at this location, Large et al. (1994) found that the seasonal cycle of SST could be well reproduced by integrating the buoy-measured surface fluxes in a K-profile parameterization (KPP) model. In this case, a nonnegligible subsurface ocean heat flux convergence was needed to keep the model SST from drifting away from climatology. This model is used in some of the experiments discussed below.

3. Data and methods

For SST information, we use the National Oceanic and Atmospheric Administration's (NOAA's) optimum interpolation sea surface temperature (OISST) dataset, version 2 (described in Reynolds et al. 2002). This dataset has weekly time resolution on a 1° grid, and is based on a mix of in situ and satellite-based SST measurements.

Five sets of net surface heat fluxes (solar and longwave radiation, and latent and sensible heat flux) are used in this study. Fluxes from reanalyses conducted using numerical weather prediction (NWP) models were obtained from both the 40-yr European Centre for Medium-Range Weather Forecasts (ECMWF) ReAnalysis (ERA-40; see Uppala et al. 2005, also available online at www.ecmwf.int) and the National Centers for Environmental Prediction–National Center for Atmospheric Research (NCEP–NCAR) reanalysis (Kalnay et al. 1996, available online at www.cdc.noaa.gov). Each of these reanalyses is available on a roughly 2.5° × 2.5° spatial grid. Daily averaged climatologies of these two datasets were used here (base periods of 1990–2004 for the NCEP–NCAR reanalysis and 1990–2002 for ERA-40, which is not available after 2002).

We also use the two Comprehensive Ocean–Atmosphere Data Set (COADS)-based (Woodruff et al. 1993; 1980–93 base period) climatologies available from the National Oceanography Centre (NOC), Southampton (available online at http://www.noc.soton.ac.uk). These are monthly mean climatologies available on a 1° spatial grid. The first set (NOC1) is produced from individual ship reports (Josey et al. 1998), and the second (NOC2) is also based on ship reports, but adjusted to have only a small annual and global mean net surface heat flux (Grist and Josey 2003). For consistency and modeling efficiency considerations, the ECMWF and NOC datasets were regridded to the grid used by the NCEP–NCAR reanalysis prior to the numerical experiments discussed below.

The fifth net surface heat flux dataset considered here is the objectively analyzed air–sea fluxes (OAFlux) for the global oceans merged dataset, which integrates satellite observations with surface moorings, ship reports, and NWP reanalysis data to determine turbulent heat fluxes on a daily 1° grid, and relies on information from the International Satellite Cloud Climatology Project (ISCCP) for the radiative fluxes (ISCCP data are interpolated to the OAFlux grid from 3-hourly and 2.5° degree resolution). OAFlux/ISCCP data are available online (http://oaflux.whoi.edu/data.html) and are described by Yu and Weller (2007). A 1990–2004 base period was used in this case.

Daily mean surface wind stress data were acquired from the Institut Français de Recherche pour l'Exploitation de la Mer (IFREMER; French Research Institute for Exploration of the Sea). This product is based on the SeaWinds/Quick Scatterometer (QuikSCAT) L2B (swath product) mean wind fields distributed by the Jet Propulsion Laboratory's Physical Oceanography Distributed Active Archive Center and uses the methods described by Smith (1988) to compute stress fields from velocity information. These data are available from July 1999 onward on a 0.5° spatial grid (available online at http://www.ifremer.fr). Daily average climatologies were formed to force the models described below. Care was taken to preserve the climatological magnitude of the wind stress in the averaging procedure. In this case, a shorter base period was used (1999–2004) because of the data availability. Some effects of uncertainty in the net wind stress applied to the models are discussed in section 6.

We also use precipitation data from the Climate Prediction Center (CPC) Merged Analysis of Precipitation (CMAP) dataset [CMAP data are provided by the NOAA/Office of Oceanic and Atmospheric Research (OAR)/Earth System Research Laboratory (ESRL)/Physical

Sciences Division (PSD), Boulder, Colorado, from their Web site at http://www.cdc.noaa.gov/]. This product is based on rain gauge information as well as satellite-based measurements and numerical model outputs (described in Xie and Arkin 1997). CMAP data are available on a 2.5° × 2.5° spatial grid. We here use the monthly mean climatology available from the Web site listed above (1979–2000 base period). Evaporation is estimated from the surface latent heat fluxes described above using a latent heat of vaporization of 2.25×10^6 J kg^{-1} and water density of 1.0×10^3 kg m^{-3}. The model results described here were found to be only subtly affected by substituting other precipitation climatologies (such as those from ERA-40 or NCEP–NCAR reanalysis). Some effects of uncertainty in the precipitation climatology are discussed below.

We also use climatological monthly mean temperature and salinity profiles from the *World Ocean Atlas 2005* (*WOA05*). This is a set of statistically interpolated fields based on in situ measurements (see Locarnini et al. 2006; Antonov et al. 2006) available on a 1° grid (online at http://www.nodc.noaa.gov). The vertical resolution of these data is 10 m from 10- to 50-m depth, 25 m from 50- to 250-m depth, and 100 m from 250- to 1500-m depth.

We mainly consider the relationship between the amplitudes of the annual harmonics of observed SST and net surface heat flux. These are determined by Fourier analysis of OISST and the various surface heat flux datasets (base periods listed above). For our purposes, the seasonal range of climatological SST is accurately approximated by twice the amplitude of the annual harmonic (cf. thick black lines in Figs. 1 and 2). For comparison with results discussed below, it is helpful to note that in the case in which mixed layer depth (h) is temporally and spatially constant, and net surface heat flux (Q^*) is wholly absorbed in the mixed layer (as would nearly be the case if annually and spatially averaged h values were considered), a simple mixed layer temperature (T) budget

$$\frac{\partial T}{\partial t} = \frac{Q^*}{c_p \rho h} \tag{1}$$

would predict similar structures for the amplitudes of the annual harmonics of SST and net surface heat flux. The heat capacity of seawater ($c_p = 2.25 \times 10^6$ J kg^{-1} °C^{-1}) and seawater density ($\rho = 1000$ kg m^{-3}) can be considered constant for the purposes of this study.

Some of the global characteristics of the annual amplitude of SST have previously been discussed by Levitus (1987), who reported that the annual harmonic accounted for the majority (usually better than 90%) of the variance

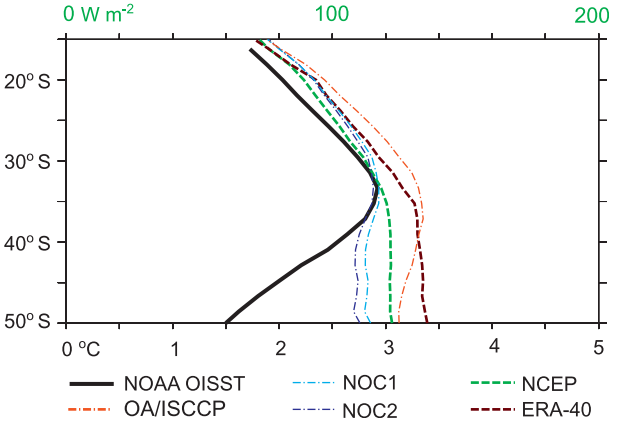

FIG. 2. Amplitude of the annual of harmonic of SST (solid black curve) and the net surface heat fluxes from the NCEP–NCAR reanalysis (green-dashed curve), ERA-40 (brown-dashed curve), the NOC1 (light blue dot–dashed curve) and NOC2 climatologies (dark blue dot–dashed curve), and the OAFlux/ISCCP dataset (orange dot–dashed curve).

of the observed annual cycle of SST (based on COADS data) over most oceanic regions, including the region discussed here. Preliminary studies for this work showed that over most of the oceanic region considered here (15°–55°S), better than 80% of the observed SST variability (inclusive of interannual variability) is accounted for by the annual harmonic of SST, based on observations from 1990 to 2004.

We report on results from arrays of two different one-dimensional ocean mixed layer models that are forced with surface fluxes of heat, momentum, and freshwater (precipitation minus evaporation), as well as a priori estimates of horizontal ocean heat flux convergence. One of these [the Price–Weller–Pinkel (PWP) model described by Price et al. (1986)], was originally used to predict SST and surface velocity variations in the Sargasso Sea. It has been used in many studies of mid-ocean SST variability, including recently the tropical and subtropical Indian (Chiodi and Harrison 2006, 2007) and Atlantic (Chiodi and Harrison 2008) Ocean. This is a now-classic model that predicts both the deepening of the mixed layer when the water column becomes either statically or dynamically unstable, and the shoaling of the mixed layer under the suitably strong addition of buoyancy to the upper layers. Dynamic mixed layer stability is based on a specified critical value of the bulk Richardson number (R_b). Gradients below the mixed layer can be smoothed out by mixing based on a critical gradient Richardson number (R_c) or the application of a uniform background diffusivity (κ). Recent studies with this model, using the same parameterization as is used here (see Table 1) have shown that, when forced with daily average NCEP–NCAR reanalysis surface

TABLE 1. Model parameters.

Model	R_b	R_c	κ	C_v
PWP	0.65	0.25	1.0×10^{-5} m^2 s^{-1}	—
KPP	0.25	0.25	1.0×10^{-6} m^2 s^{-1}	1.5

heat fluxes, this model is capable of accurately (to the first-order levels considered here) reproducing the amplitude of the annual harmonic of SST in much of the north tropical and subtropical Atlantic (see Chiodi and Harrison 2008).

The second ocean model used here is the KPP model described by Large et al. (1994). This model was developed for use in climate models and predicts diffusivity in the surface ocean boundary layer, where surface flux–driven processes cause mixing at levels higher than those seen in the ocean interior. The KPP model also includes parameterizations for (smaller) diffusivities in the ocean interior caused by internal wave breaking (constant), shear instability (Richardson number based), and double diffusion (not included in our standard runs). Similarly to the PWP model, this model predicts the depth of the surface boundary layer based on a critical bulk Richardson number [see Large et al. (1994) for a complete model description]. The version of the KPP model used here (see Table 1 for the parameterization) was able to accurately predict the amplitude of the seasonal cycle of SST at OWS Papa to within a few percent of the observed value when forced with the observed local surface fluxes, consistent with the results originally discussed by Large et al. (1994) for both the KPP and PWP cases; our philosophy is to use the same parameterizations at each location so that regional differences in model performance can be more easily determined.

In each system, model arrays span the oceanic region between 15° and 50°S, on a roughly 2.5° × 2.5° grid; grid points that either contain or are adjacent to ''land'' grid points are not considered to alleviate possible problems with determining air–sea fluxes in these regions (see Kara et al. 2007). Initial conditions are taken from annual mean salinity and temperature profiles from the *WOA05* dataset. Experiments have shown that the results discussed here are rather insensitive to changes in initial conditions, as long as they are reasonable (e.g., using July rather than annual mean initial conditions, with an area-averaged change in initial SST of about 1.5°C, results in only small changes in predicted annual harmonic amplitude; see the appendix). Each model uses the same linearized version of the equation of state based on the observed annual average surface temperature and salinity. Experiments using the full equation of state at each vertical grid point (not shown) were found to be qualitatively similar to the results discussed below (see the appendix). Vertical shortwave extinction coefficients were based everywhere on a Jerlov-type IA water mass for simplicity (Jerlov 1976). Trials using other water types, with similar properties (e.g., Jerlov I or Jerlov II), produced qualitatively similar results. Integrations were carried out for a total of 3 yr, starting in winter (1 July), though only results from the first 1 January–31 December period are discussed. The remaining years are used here only to estimate the annual temperature trend (discussed below), though each of the model years were found to produce similar results.

In our model runs, the temperature tendency resulting from Ekman-type meridional ocean heat flux convergence was added to the mixed layer. This practice is consistent with results reported by several studies of the Southern Ocean's upper-ocean heat budget, which suggest that regionally averaged net surface heat flux is mainly balanced by Ekman current–driven oceanic heat flux convergence (see Sallee et al. 2006; MacCready and Quay 2001; Rintoul and England 2002). Only the meridional Ekman component was added because preliminary analysis showed that temperature tendencies resulting from geostrophic and zonal Ekman currents were generally negligible compared to the meridional Ekman component. Similar findings are reported by Dong et al. (2007); as has been established elsewhere (Dong et al. 2007), we estimate this tendency as

$$\frac{\partial T}{\partial t} = -\mathbf{V} \cdot \frac{\partial T}{\partial y}, \tag{2}$$

where $\mathbf{V}$ is meridional current and $\partial T/\partial y$ is the meridional temperature gradient. Here, $\mathbf{V}$ is determined using QuikSCAT wind stress, assuming that wind stress is absorbed entirely in the mixed layer. In this case, the SST gradient is based on OISST data and the mixed layer depth is estimated by the numerical models described below. Zonally and annually averaged, this term shows a peak of roughly 1×10^{-5}°C m s^{-1}, between 45° and 50°S and crosses zero between 30° and 35°S (Fig. 3). We also experimented with calculating this term from other wind stress climatologies (e.g., ERA-40 and NCEP–NCAR reanalysis) and from currents produced by the Simple Ocean Data Assimilation (SODA) version 1.4.2 (Carton et al. 2000), which includes geostrophic components, but we found that neither substituting currents from other wind stress datasets nor using the SODA-based currents qualitatively affected the results discussed here (see the appendix). Running the model without this term, however, results in significantly (unrealistically) increased amplitudes in the higher latitudes considered

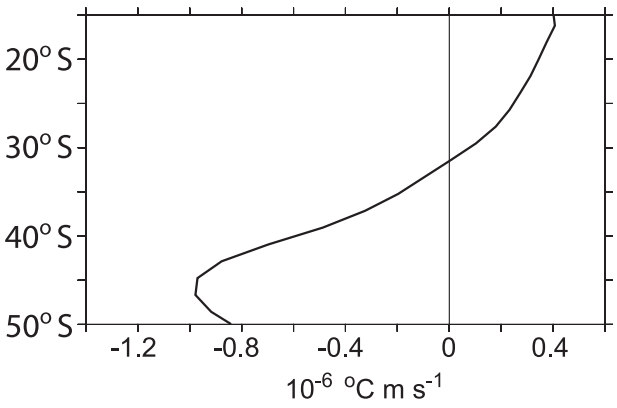

FIG. 3. Mixed layer temperature tendency; zonal average of $-\tau/\rho f \cdot \partial T/\partial y$ (black curve) based on QuikSCAT derived wind stress (τ) and OISST (T) is shown; ρ is seawater density and f is the Coriolis parameter.

(not shown), where the combination of relatively strong winds and large meridional SST gradients makes this term a significant contributor to the mixed layer heat budget.

Despite the inclusion of wind-driven horizontal ocean heat flux convergence, model results often show unrealistic trends, the sign and magnitude of which are dependent on location. Such imbalances can stem from errors in the surface heat fluxes, ocean heat advection, and diffusion effects and possibly unresolved or improperly parameterized model processes. The majority of these model trends are within the accuracy with which the heat budget of the Southern Ocean can be closed using contemporary observations; for most runs, 90% of the ocean grid points at each latitude have trend magnitudes less than 1.1×10^{-7}°C yr^{-1} (cf. Dong et al. 2007). Even so, balancing this amount of heat can have nonnegligible effects on model results if done in a manner that alters stratification, as might be the case if the heating or cooling needed to balance the heat budge was substantial in magnitude and was added primarily at one (or a few) vertical level(s). Alternatively, the trend may be taken out by specifying a more vertically uniform heating or cooling. We find that results obtained by balancing the heat budget with vertically uniform heat flux are virtually identical to those from runs in which no flux correction is made and a linear trend is removed (if present) from the model results before calculating the amplitude of the annual harmonic of SST (see the appendix). We mainly consider results from this last model configuration because it gives results that are equivalent to the more computationally expensive uniform flux correction runs, and results are controlled purely by the specific combinations of model physics and heat flux datasets considered; that is, we avoid making flux adjustments that influence results but are unwarranted by observational evidence.

Results from models that are integrated with climatological surface fluxes, such as those considered here, are not affected by possible correlations between interannual anomalies in the surface fluxes and mixed layer depth. Effects from such correlations on the seasonal cycle resulting from Reynolds-type averaging can be estimated from actual time series of fluxes and mixed layer depths; however, determining a multiyear record of basin-scale mixed layer depth is beyond the scope of this work. These effects, however, are expected to be small compared to the differences seen between results using different flux datasets (discussed below). In preliminary experiments, the daily average forcing was integrated in some of the models considered here over several years (so results include these effects), but differences between annual SST amplitude results from these runs and ones using climatological forcing were found to be small (and generally of the opposite sign) compared to the model-to-observation biases (see the appendix).

There are generally two ways to construct mixed layer depth climatologies: one can either average over mixed layer depths obtained from individual temperature and salinity profiles, or first average the profile data, and then determine mixed layer depth. For comparison, we consider observational mixed layer depth information from both methods. First, we use the monthly climatological temperature and salinity profiles in *WOA05* (interpolated to 1-m vertical resolution) to estimate mixed layer depth, which in this case is defined as the depth at which subsurface density exceeds density at 10-m depth by a value of 0.125 kg m^{-3}, as is standard for this type of dataset. Also, mixed layer depths determined from individual profiles according to the methods discussed by de Boyer Montégut et al. (2004; depth where the density increase compared to density at 10-m depth equals 0.03 kg m^{-3}) are considered (data available online at http://www.locean-ipsl.upmc.fr/~cdblod/mld.html; this currently includes Argo profiling float data up to September 2008). Other mixed layer depth climatologies of both types are available (e.g., Lorbacher et al. 2006; Kara et al. 2000; Monterey and Levitus 1997) but mainly are not considered here because they depend on previous period datasets that do not benefit from recent increases in sampling frequency at the higher latitudes considered (as discussed below).

For comparison purposes, the model mixed layer depths were determined as the depths of the first vertical grid point with a density jump greater than 0.01 and 0.0001 kg m^{-3} above the surface value, for the KPP and PWP models, respectively. The larger value used in the KPP case was determined based on visual inspection of

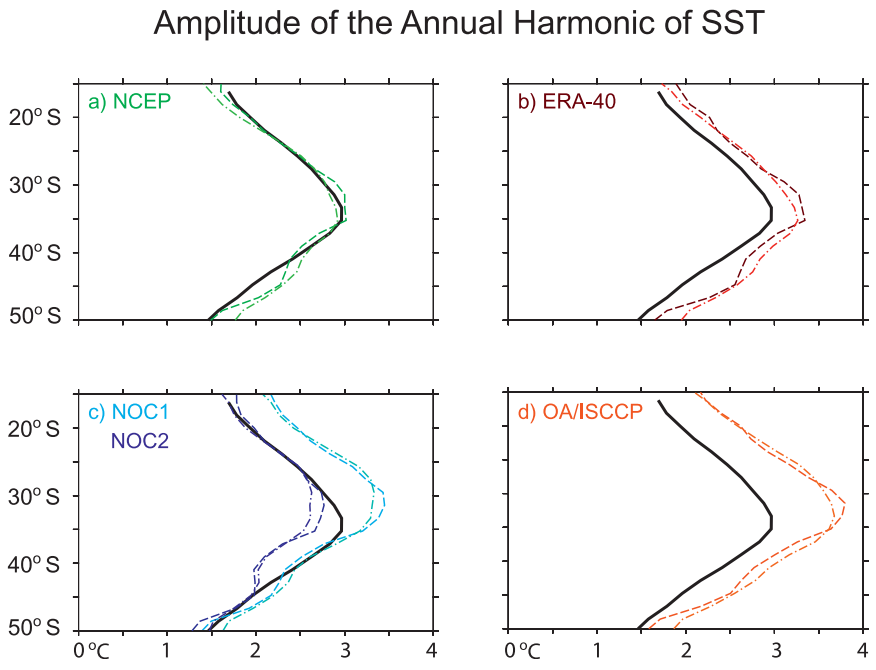

FIG. 4. Zonal averages of the amplitude of the annual harmonic of SST. The result from observations (NOAA OISST) is drawn (solid black curve). Results from the simple analytical model described by Eq. (1) integrated with net surface heat flux from the (a) NCEP–NCAR reanalysis, (b) ERA-40, (c) NOC1 and 2, and (d) OAFlux/ISCCP climatologies are drawn (color, as labeled), as are results using *WOA05* (dashed curve) and the de Boyer Montégut (2004) (dot–dashed curve) mixed layer depth climatologies.

profiles at each latitude considered, and is a reflection of the fact that the KPP model allows small vertical gradients of tracers within the surface boundary layer, whereas the PWP model, by design, completely mixes tracers within the mixed layer. We note, however, that these values do not affect the model integrations themselves, and the affects on our analyses caused by using different values in the 0.1–0.0001 range do not qualitatively affect the results presented here.

4. Amplitudes of the annual harmonic of SST predicted from observed mixed layer depths

The results presented in this section show that the general meridional shape, and, in some cases, the absolute value of the observed zonally averaged amplitude of the annual harmonic of SST, can be well reproduced by Eq. (1) when h is specified as a function of space and time according to *WOA05* or de Boyer Montégut et al. (2004) data. Penetrative incoming solar radiation is accounted for, such that $Q^* = Q - Q_p$, where Q is the net incoming surface heat flux and Q^* is the portion absorbed in the mixed layer and Q_p is the penetrative portion (determined from the Jerlov IA vertical extinction coefficients and mixed layer depth). For each set of surface fluxes, two integrations were carried out: one using the *WOA05*-based estimate of the mixed layer depth and another using the de Boyer Montégut et al. estimate. Results based on mixed layer depths using previous versions of the *World Ocean Atlas* data [e.g., *WOA01* (Stephens et al. 2002; Boyer et al. 2002); results not shown] and the Lorbacher et al. (2006) dataset (which depends on pre-2002 data) were unable to accurately reproduce observations at the higher latitudes considered, suggesting that the recent increases in sampling frequency have substantially improved our knowledge of this region of the ocean.

Results obtained by integrating each of the surface fluxes in Eq. (1) roughly reproduce the general shape of the observed results (see Fig. 4). The two mixed layer depth climatologies used here tend to produce similar results, though some of the surface flux datasets do better than others. Results obtained using the NCEP–NCAR reanalysis surface heat fluxes come the closest to observations; for both mixed layer depth cases, zonally averaged amplitudes of the annual harmonic of SST deviate by no more than about 0.25°C in the region considered, and there is only a very small averaged bias (less than 0.05°C averaged over 15°–50°S). The ERA-40 surface heat flux–based results also accurately reproduce the

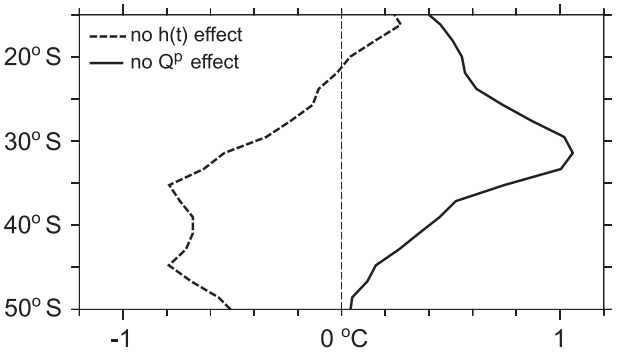

FIG. 5. Zonally averaged bias (adjusted result minus original result) caused by neglecting the effects of the penetration of solar radiation (solid curve) and by replacing the mixed layer depth $h(x, y, t)$ in Eq. (1) with its temporal average (dashed line). Each result above is based on the NCEP–NCAR reanalysis and *WOA05* mixed layer depth integration (see text).

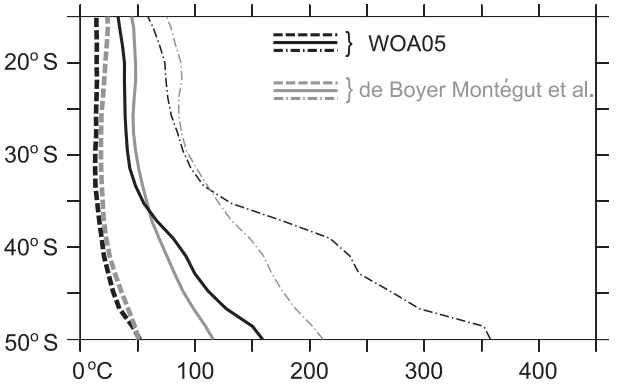

FIG. 6. Progressively deeper curves are the zonally averaged monthly minimum (dashed curves), annual mean (solid curves), and monthly maximum (dot–dashed curves) mixed layer depths from the *WOA05* (black curves) and de Boyer Montégut et al. (2004) (gray curves) climatologies.

shape of the observed results, although they are biased toward larger amplitudes by about 0.5°. The OAFlux/ISCCP results are also biased toward larger-than-observed amplitudes, showing biases similar to ERA-40 results in the higher latitudes but more severe biases in the 15°–35°S latitude band. Comparison of the NOC1 and NOC2 cases indicates that the adjustments made to the NOC2 fluxes have the effect of reducing the zonally averaged amplitude at all latitudes and changing the character of the their relationship to observations; the NOC1 results are closer to the observations in the higher latitudes than in the lower ones, where they are biased high, whereas the NOC2 results are closer to observations in the lower latitudes than in the higher latitudes, where they are biased low.

It is notable that both NCEP–NCAR reanalysis flux–based results are reasonably close to the observed values throughout the entirety of the region considered and predict the latitude of the maximum zonally averaged amplitude to within about 5°.

The results of this simplified analysis provide useful insights into the processes that control the observed structure of the amplitude of the annual harmonic of SST. The reasonable agreement between these results (especially the NCEP–NCAR reanalysis flux case) and observations suggest that, to first-order accuracy, the observed behavior of the seasonal cycle of SST, and therefore most of the observed variability of SST in the region considered, is explained by physical processes described in Eq. (1). Furthermore, the fidelity of these results suggests that processes that are neglected by Eq. (1) either have small or compensatory effects on the seasonal cycle of SST. From this perspective, it is necessary to consider mainly two sets of oceanic processes to understand most of the observed SST variability—the penetration of solar radiation in seawater and the processes that control the spatial and temporal variability of the mixed layer depth.

The first of these depends upon the composition of seawater, and though it is known to depend in detail upon the amount and type of particulate matter found in the upper (roughly surface to 20-m depth) water column, the results discussed above suggest that considering light penetration as a spatially uniform process is adequate for the purposes of this study.

Zonally averaged SST amplitudes estimated by neglecting solar penetration ($Q_p = 0$) retain the cone-shaped character of the observations, but are generally biased toward higher-than-observed amplitudes (the zonally averaged bias is shown in Fig. 5 for the NCEP–NCAR reanalysis and *WOA05* mixed layer depth case). This bias is largest around 35°S (about +1.2°C), and smallest near 50°S. This is because the effect of unrealistically absorbing all solar radiation in the mixed layer is largest where the summertime mixed layers are shallowest (cf. summertime values in Fig. 6).

Perhaps the more relevant implication of the results shown in Fig. 5 is that the temporal and spatial variability of the mixed layer depth is primarily important to the character of the observed seasonal cycle of SST. Examination of zonal averages of the observed climatological annual mean mixed layer depth (Fig. 6) shows that the annual mean mixed layer depth (solid curves) stays relatively constant from about 16° to 34°S, but deepens more or less linearly from about 65-m depth at 35°S to about 120- or 160-m depth at 50°S, depending on the climatology considered. Despite the apparent discrepancies between datasets, each shows that with higher latitude, there is more mass to heat up and cool down in the mixed layer in an annually averaged sense. Therefore, the surface

temperature becomes significantly less sensitive to surface forcing variability at higher latitudes. Our experiments show, however, that the temporal variability of the mixed layer depth is also important; when the temporally varying h in Eq. (1) is replaced with its annual mean value, the integration of Eq. (1) predicts an annual SST amplitude that is too low in the middle and higher latitudes (the bias is shown as dashed line in Fig. 5). Thus, the temporal variability (e.g., shoaling of the mixed layer in the summer) tends to increase the observed annual SST amplitude, in a zonally averaged sense, over most of the region considered. This effect is largest near the peak at about 35°S (see Fig. 5), where some of the shallowest summertime mixed layer depths occur. Comparison of the zonally averaged monthly minimum (dashed curve) and monthly maximum (dot–dashed) mixed layer depths shows that there is better agreement between these two datasets in the warm season than the cold season. Because there is good agreement between the ranges of SST predicted from these two datasets (cf. Fig. 4), we can infer that the annual range of SST is more sensitive to differences in summertime than wintertime mixed layer depth values.

The results presented in this section have informed the design of the experiments discussed below, in that they suggest that the physics that are necessary to predict a reasonably accurate annual cycle of SST are relatively simple; a model that reasonably predicts the mixed layer depth (especially during the warm season), so long as other processes are not too unrealistic, should also reasonably predict the annual cycle of SST. Next, we determine the degree to which the prognostic mixed layer models described above are able to do this when forced with the fluxes considered here.

5. Ocean mixed layer model results

To test the degree to which the mixed layer depths predicted by the models used here are consistent the *WOA05*-based results described above, we have integrated Eq. (1) using the mixed layer depths from both the PWP and KPP standard model runs. Although the model runs include other processes (e.g., entrainment, vertical temperature diffusion) that are not resolved by Eq. (1), we have chosen to look at the results through the lens of Eq. (1), because observational estimates of the climatological effects of these other processes are generally sparse and difficult to obtain, whereas the results presented above show that *WOA05*-based mixed layer depth data provide a useful guideline for model comparison.

a. The PWP model

In the PWP case, all of the integrations generally predict amplitudes that are higher than those observed and higher than the respective *WOA05* cases. The worst offenders are the ERA-40, NOC1 (nonadjusted), and OAFlux/ISCCP cases, which severely overpredict the amplitude of the annual harmonic of SST over most latitudes, and especially in the midlatitudes (see Fig. 7a). These three cases also generally underpredict the observed mixed layer depth the most (see Figs. 7b–d), including in the summer, when the mixed layer depths predicted by the ERA-40 and NOC1 runs are shallower than the *WOA05* and de Boyer Montégut et al. (2004) summertime estimates by more than a factor of 2 near 35°S. The biases caused by these unrealistically shallow mixed layers are also compounded by the fact that, in each case, more of the annually varying component of net surface heat flux (not shown) is absorbed in the mixed layer than in the NCEP–NCAR reanalysis or NOC2 cases.

The PWP NCEP–NCAR reanalysis– and NOC2-based results show a similar variation of amplitude with latitude (solid gray and dash–dotted gray curves in Fig. 7). Each is generally biased toward higher-than-observed amplitudes, with the largest discrepancy appearing at the higher latitudes, where the model bias toward lower-than-observed mixed layer depth is greatest. Because, in each case, this model is unable to adequately recreate the observed structure of the annual SST amplitudes, we conclude that this model system is either too strongly deficient (e.g., some model physics are missing) or contains too many errors (e.g., none of the sets of surface fluxes are sufficiently accurate) to explain the observed structure of the annual cycle of SST. We will discuss the sensitivity of the results to some possible adjustments of the model system below.

b. The KPP model

The biases of the KPP-based results have a different character than those of the PWP-based system, although, upon close inspection, some similarities between these two systems can be found (see Fig. 8). With the exception of the NOC2 case, over most latitudes the KPP-based results are biased toward higher-than-observed SST amplitudes (like the PWP case). This occurs despite the fact that the KPP-based system predicts mixed layer depths that are, on average, mostly deeper than the *WOA05* results. This is a result of the strongly nonlinear nature of Eq. (1), which is caused by the $1/h$ term. With deeper mixed layers in the KPP case, the biases of the ERA-40- and NOC1 (unadjusted)-based results are not as profound as those in the PWP case. The biases in these two KPP cases are still significant, however, with values up to about 1.5°C for each. The NCEP–NCAR reanalysis–based SST amplitudes can be described as moderately consistent in character to the observational results (within about 0.5°C and having a similar meridional shape) over much of the region considered (about 20°–42°S), but they

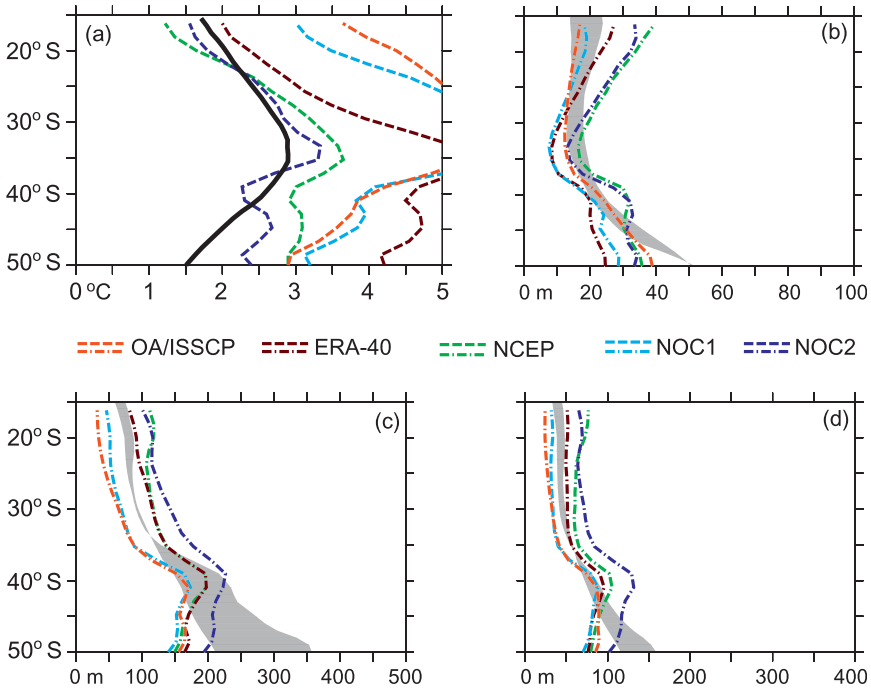

FIG. 7. (a) Amplitude of the annual harmonic of SST based on NOAA OISST (solid black curve) and integration of Eq. (1) using NCEP–NCAR reanalysis fluxes and mixed layer depths from a run of the PWP model integrated with NCEP–NCAR reanalysis (green-dashed curve), ERA-40 (brown), NOC1 (light blue), NOC2 (dark blue), and OAFlux/ISCCP (orange) surface heat fluxes. The zonally averaged (b) minimum monthly averaged, (c) maximum monthly averaged, and (d) annual mean mixed layer depths from each of the integrations shown in (a). Shading is between the respective *WOA05* and de Boyer Montégut et al. (2004) observation-based mixed layer depth results (see Fig. 4).

fail to predict adequately small amplitudes in the higher latitudes. This high-latitude discrepancy can be attributed mainly to the failure to predict deep summertime mixed layers adequately (see Fig. 8a) because the $1/h$ term in Eq. (1) makes results highly sensitive to shallow summertime biases.

The NOC2 case predicts the smallest zonally averaged amplitude in most of the region considered (roughly 25°–50°S). Here, it also predicts the deepest mixed layer depth and has the smallest surface heat flux annual amplitude to begin with (cf. Fig. 2). Thus, the confluence of these two factors appears to bias this run toward generally smaller-than-observed amplitudes, unlike the rest considered. Interestingly, even this run underpredicts the summertime mixed layer depth in the higher latitudes resolved (south of about 45°S); this is also the only region where this run overpredicts the annual amplitude, albeit slightly.

6. Model sensitivity to annual mean surface forcing

Given the inherent uncertainty in the surface forcings themselves, it is useful to determine the effects that changes in these forcings have on model results. To do this, we discuss perturbation experiments in which the annual-mean surface fluxes (wind stress, heat flux, and precipitation minus evaporation) were separately adjusted at each model grid point.

For the first set of experiments, perturbations were chosen randomly from a uniform distribution, with the range set to approximately ±2 times the average zonal standard deviation of the respective curves shown in Fig. 9.

Results of these experiments (Fig. 10) show that perturbations applied to net heat and momentum fluxes can have significant effects on model results. For the vast majority of points, the model perturbations are as expected from consideration of the $1/h$ term in Eq. (1); increases in net (downward) momentum flux and upward heat flux increase mixed layer depth and, therefore, decrease SST amplitude. The roughly opposite effect holds for decreases in net momentum and upward heat flux. For each term, changes in amplitude of up to about 1°C (1.5°C in the KPP heat flux case) are observed when the perturbations are near their prescribed limits. It is clear from the scatter among points shown in Fig. 10, however, that results depend on location.

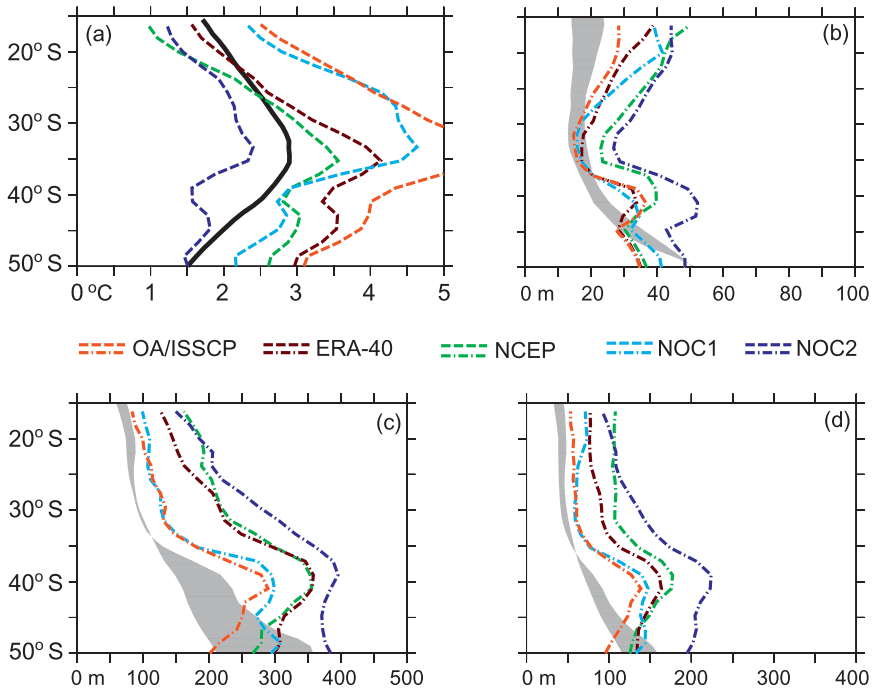

FIG. 8. Same as Fig. 7, but using the KPP model.

In the case of precipitation variations, the effects are about a factor of 3 smaller than those seen in the heat and momentum flux cases, though they are still as expected from consideration of Eq. (1); all things being equal, the addition (removal) of freshwater to (from) the surface generally causes shallower (deeper) mixed layers to form and, thus, increases (decreases) the amplitude of the annual harmonic of SST.

The results presented in this section can be used to explain some of the differences seen in the model results discussed above (cf. Figs. 7 and 8); for example, the NOC2 fluxes drive the smallest SST amplitudes seen south of about 25° in each set of model results (KPP and PWP). The results of this section suggest that this can largely be explained by the relatively large out-of-ocean net surface heat flux estimates seen in the NOC2 case (cf. Figs. 7–9).

The possibility of ''nudging'' the model-predicted annual SST amplitudes and mixed layer depths toward observed values by making reasonable (e.g., within estimated uncertainty) adjustments to the surface fluxes was considered. However, results appear to show little chance for accurately predicting both of these key oceanic variables simultaneously by this means. This was determined by first estimating the change in a given oceanic variable (e.g., SST amplitude, monthly mean, or minimum mixed layer depth) with respect to changes in a given surface flux component at each location through a series of model perturbation experiments. Ostensibly, the flux adjustment values necessary to correct model errors in two (or three) variables then can be found. For example, the system

$$\frac{\partial A}{\partial Q}\cdot\Delta Q+\frac{\partial A}{\partial \tau}\cdot\Delta\tau=\Delta A \tag{3}$$

$$\frac{\partial h_1}{\partial Q}\cdot\Delta Q+\frac{\partial h_1}{\partial \tau}\cdot\Delta\tau=\Delta h_1 \tag{4}$$

can be solved for flux adjustments ΔQ and $\Delta\tau$, given errors in annual SST amplitude (ΔA) and mean monthly mixed layer depth (Δh_1), and the partial differentials $\partial A/\partial Q$, $\partial A/\partial\tau$, $\partial h_1/\partial Q$, and $\partial h_1/\partial\tau$ (determined from the model results described above). Some issues arise when attempting to do this, however. Notably, the matrix formed by the partial differentials above is ill conditioned in the vast majority of the locations considered [97% and 99% have a condition number >100, in the PWP and KPP cases, respectively, and most are more than a factor of 10 worse than this; well-conditioned matrices have condition number near unity (see Leon 1994, 395–400)]. Other combinations of two or three flux adjustments and predicted model variables are possible (e.g., using precipitation adjustments and/or minimum monthly mixed layer depth), but all of the combinations of the variables discussed here were examined and found to be as bad or worse than this example. Though not a surface flux, effects of adjusting the prescribed background model diffusivity were also considered, but, like the surface flux effects, these were found to be

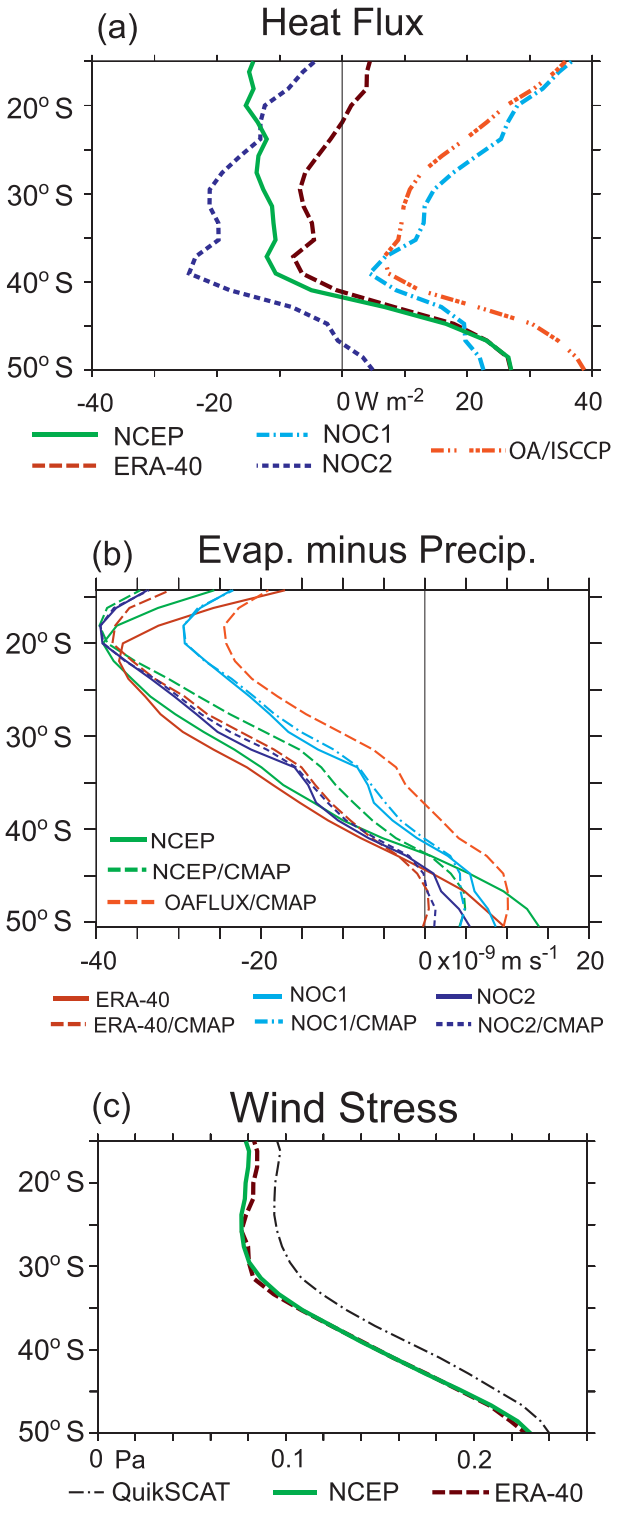

FIG. 9. Zonal, ocean-only averages of (a) Annual mean surface heat flux (positive for ocean heat gain), (b) annual mean evaporation minus precipitation ($E - P$), and (c) annual mean surface wind stress. For $E - P$, results based on CMAP precipitation are drawn with dashed curves. Respective dataset precipitation is used otherwise, if available (solid curves; as listed.).

unsatisfactory for the purposes discussed here. Physically, the reason for this is that the relative effects of the subsequent flux adjustment (e.g., wind stress) on the model-predicted variables are either insufficient or too similar to the effects of the first adjustment (e.g., heat flux) to provide an independent control of the subsequent (e.g., mixed layer depth) model-predicted variable. In all cases, the magnitudes of the flux adjustments determined from these methods were found to be mostly larger (e.g., about 85% of grid points with Q or τ exceeding 100 W m^{-2} or 0.05 Pa, respectively) than those that can be reasonably argued for based on the uncertainty in the flux estimates. Trials with individual model runs have confirmed these results. Thus, among the mixed layer models and forcing datasets considered, we are unable to find a configuration that reasonably reproduces observed mixed layer behavior in the higher latitudes considered.

7. Discussion and conclusions

All of the datasets considered show that, when averaged zonally over the oceanic regions of the Southern Hemisphere, the amplitudes of the annual harmonic of net surface heat flux in the higher latitudes considered (40°–50°S) are nearly as large (no less than 5% smaller) or larger than the amplitude found near 35°S. Despite this, the zonally averaged annual range of Southern Hemisphere SST peaks at about 35°S, and decreases substantially poleward of 35°S. This means that substantial changes that in upper-ocean dynamics must occur with latitude to account for the observed annual cycle of SST.

Simple integrations that consider just the effect of surface heat flux on the ocean mixed layer temperature tendency can reasonably account for the observed climatological behavior of SST when the mixed layer depth information is based on contemporary observations. In these models, it is the spatial and temporal variation of the mixed layer depth that primarily causes the falloff of the annual range of SST at higher latitudes. From the oceanic perspective, results show that predicting accurate annual ranges of SST in such models depends more on reproducing accurate summertime behavior and correctly timing the seasonal shoaling/deepening of the mixed layer than on reproducing absolute wintertime mixed layer depth values. We suggest that the mixed layer depth variability observed in contemporary climatologies be used as a guideline for ongoing climate model development.

To test whether some currently used prognostic mixed layer models are capable of adequately reproducing this type of mixed layer depth variability, we integrated several sets of surface heat fluxes in such models. The fidelity of these results to observations varies considerably depending on the latitude considered. Remarkable

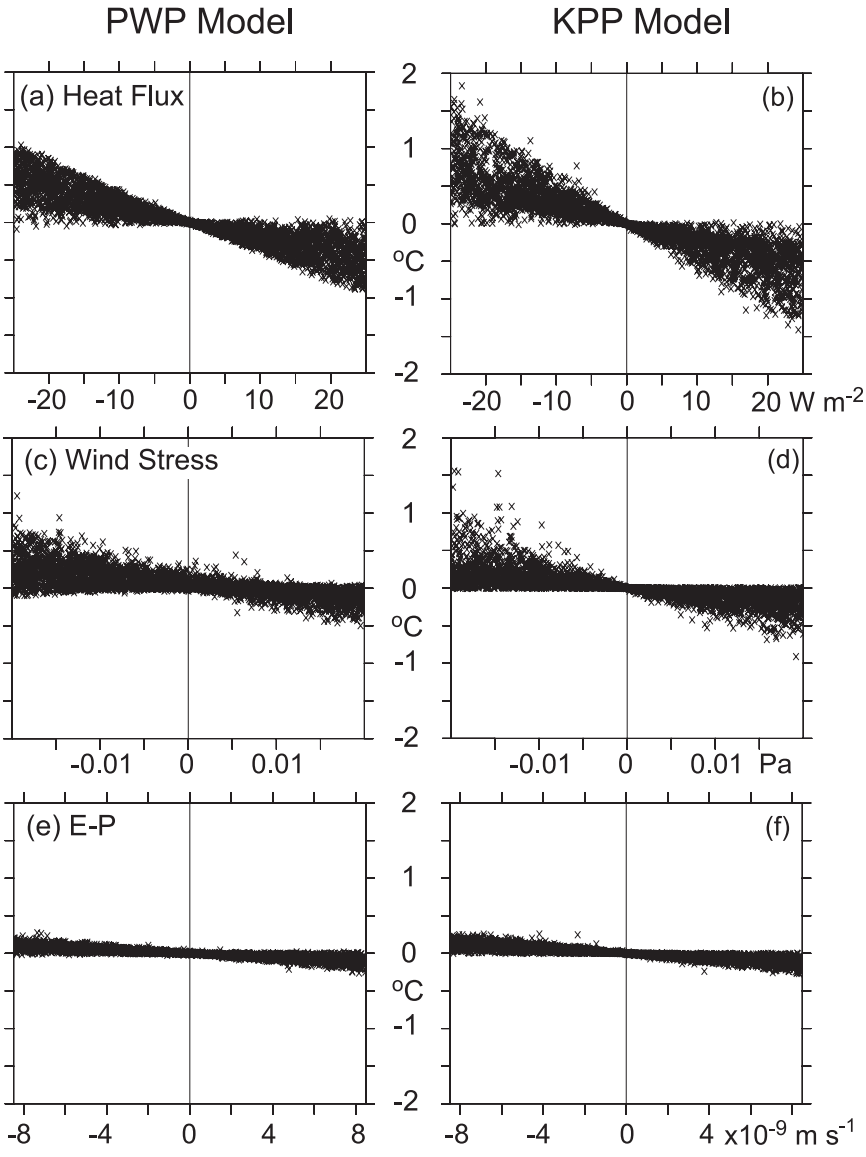

FIG. 10. Scatterplots of the change in amplitude of the annual harmonic of SST vs perturbation. In this case, the perturbations are time-invariant changes in the annual mean net surface flux and SST is reconstructed using Eq. (1). Results are for (a) heat flux in PWP, (b) heat flux in KPP, (c) wind stress in PWP, (d) wind stress in KPP, (e) evaporation minus precipitation ($E - P$) in PWP, and (f) $E - P$ in KPP.

agreement is seen in many cases in the subtropics and midlatitudes, confirming the utility of the prognostic models in these regions. Results at higher latitudes, however, show considerable biases, which are dependent on the choice of the model and the surface flux dataset. For a given surface flux dataset, the KPP model generally predicts a smaller annual range of SST and a deeper mixed layer depth than the PWP model. Because most all of the results, irrespective of model choice, are biased toward higher-than-observed annual SST ranges on average in the mid- and high-latitude regions, the KPP model may appear to be more accurate; however, the KPP model achieves this result partly by overpredicting the annual mean mixed layer depth for most of the latitudes considered. Thus, we find that, in the configurations used here, neither model properly reproduces the seasonal variability of the upper ocean at high southern latitudes. Particularly, it is notable that the rather smooth progression toward deeper mixed layer depths with increasing latitude from about 35° to 50°S that is seen in both sets of observations considered here is lacking in the prognostic model results, which instead tend to show little

overall deepening of the mixed layer from about 40° to 50°S.

Despite repeated efforts to do so, we were unable to substantially improve model performance by adding previously identified processes to the model configurations used here (many results are described in the appendix). For example, adding ocean heat flux convergence based on currents from the SODA dataset, which includes effects of geostrophic currents, produces results that are not much different than those obtained using only the wind-driven component.

Though unlikely to account fully for model-to-observation discrepancies discussed above, consideration of the effects of nonzero annual mean net surface heating does suggest that a possible contributing factor to the falloff of annual SST range is that a destabilizing amount of its heat is lost annually from the ocean surface at higher latitudes. To the extent that this effect dominates those from unresolved processes that are needed to balance the heat budget, this highlights a possible important connection between meridional oceanic heat transport and the annual range of SST. The net surface heat fluxes shown in Fig. 9a range from being mostly out of the ocean (NOC2) to entirely into the ocean (NOC1; OAFlux/ISCCP). Because meridional oceanic heat transport can be determined by integrating net surface heat flux, this discrepancy corresponds to significant differences in the meridional oceanic heat transport; if the observed value of about −0.5 PW at 32°S, reported by Ganachaud and Wunsch (2000), is used as a benchmark, these differences correspond to the difference between net northward (NOC2 case) and net southward (all other cases) meridional heat transport at the higher latitudes considered. Unfortunately, the true nature of this transport in the Southern Ocean is currently a matter of debate (cf. Grist and Josey 2003; Ganachaud and Wunsch 2003), but the results presented here show that progress in understanding either the mechanisms responsible for the annual range of SST, or the character of oceanic heat transport can inform current efforts to better understand the other.

A quick look at results from the coupled climate model integrations that have been conducted in support of the recent Fourth Assessment Report from the International Panel on Climate Change (IPCC AR4; Meehl et al. 2007) shows that, like the simple models considered here, most of the IPCC AR4 models predict an annual range of SST that is too large in the higher latitudes considered here; the ensemble mean annual range of SST (twice the annual amplitude) from the 22 IPCC AR4 results shown in Fig. 11 is about 1.5°C larger than that observed at 50°S, and about 2°C larger than that at 55°S. Although the observed range is more closely reproduced by many of the IPCC AR4 models than the mixed layer models use here, results from the PWP and KPP models are within the IPCC AR4 range when forced with the NCEP–NCAR reanalysis surface fluxes (based on root-mean-square error the KPP and PWP results rank 19th and 20th, respectively, out of the 24 model results shown in Fig. 11). This suggests that current coupled climate modeling efforts may benefit

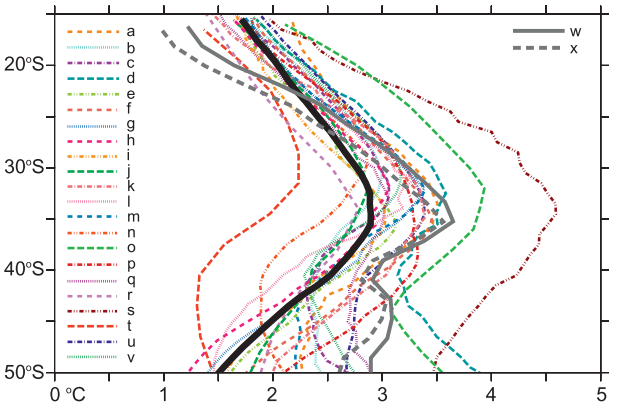

FIG. 11. Zonally averaged amplitude of the annual cycle of SST from observations (thick solid black curve) and from the models contributed in support of the IPCC AR4 preindustrial control experiment. Model results are as follows: (a) Beijing Climate Center (BCC) Coupled Model, version 1 (CM1; rank 15); (b) Canadian Centre for Climate Modelling and Analysis (CCCma) Coupled General Circulation Model, version 3.1 (CGCM3.1), T47 resolution (rank 9); (c) CGCM3.1 T63 resolution (rank 11); (d) Centre National de Recherches Météorologiques Coupled Global Climate Model, version 3 (CNRM-CM3; rank 22); (e) CSIRO Mk3.0 (rank 2); (f) CSIRO Mark, version 3.5 (Mk3.5; rank 12); (g) Hadley Centre Global Environmental Model, version 1 (HadGEM1; rank 5); (h) HadCM3 (rank 4); (i) CCSM3 (rank 1); (j) MRI CGCM2.3.2 (rank 3); (k) ECHAM and the global Hamburg Ocean Primitive Equation (ECHO-G; rank 13); (l) Model for Interdisciplinary Research on Climate 3.2, high-resolution version [MIROC3.2(hires); rank 8]; (m) MIROC3.2 medium-resolution version [MIROC3.2(medres); rank 7]; (n) L'Institut Pierre-Simon Laplace Coupled Model, version 4 (IPSL CM4; rank 10); (o) Institute of Numerical Mathematics Coupled Model, version 3.0 (INM-CM3.0; rank 23); (p) Istituto Nazionale di Geofisica e Vulcanologia (INGV) SINTEX-G (SXG; rank 17); (q) Flexible Global Ocean–Atmosphere–Land System Model, gridpoint version 1.0 (FGOALS-g1.0; rank 16); (r) GISS-ER (rank 6); (s) Goddard Institute for Space Studies Model E-R (GISS-EH; rank 24); (t) Goddard Institute for Space Studies Atmosphere–Ocean Model (GISS-AOM; rank 21); (u) Geophysical Fluid Dynamics Laboratory Climate Model, version 2.0 (GFDL CM2.0; rank 14); and (v) GFDL Coupled Model, version 2.1 (CM2.1; rank 18). See PCMDI documentation for more information on these models (onrank at http://www-pcmdi.llnl.gov). Curves (w) (rank 20) and (x) (rank 19) show the NCEP-based results from Figs. 7 and 8, respectively, for comparison. The ranking given to the preceding list of 22 AR4 and 2 ocean mixed layer model is based on the root-mean-square error between the observed and respective model results (best-fit first).

from efforts to improve and better understand the behavior of ocean mixed layer model configurations, such as those considered here. It is interesting that a few IPCC AR4 results show rather close agreement with observations in this respect [especially the Community Climate System Model, version 3 (CCSM3), Commonwealth Scientific and Industrial Research Organisation Mark version 3.0 (CSIRO Mk3.0), Meteorological Research Institute Coupled General Circulation Model, version 2.3.2a (MRI CGCM2.3.2), and Met Office third climate configuration of the Met Office Unified Model (HadCM3) cases]. We suspect that a detailed analysis and comparison of the various surface forcings and model parameterizations in the IPCC AR4 archive (several of which use the KPP model) may provide a better understanding of the mechanisms controlling mixed layer depth variability in the higher latitudes considered here. We leave such analysis for future work.

The mixed layer modeling efforts of this study show that the models considered are by no means constrained to reproduce very accurate climatological results at high latitudes in the Southern Hemisphere by our current understanding of model physics and heat and momentum fluxes. Though errors in the fluxes beyond those considered here can contribute to this, the relative sensitivity of the results to flux adjustments considered and the breakdown of realistic model mixed layer behavior at high latitudes suggests to us that the suite of physics resolved by these models fails to adequately resolve some physical processes at higher latitudes. In either case, more work is necessary on the part of both modelers and observers to improve our understanding of the processes governing the behavior of this region of the World Ocean.

Because of the climatological effects that this region of ocean has on neighboring land and (at higher latitudes) ice-covered regions, much of the world's climate would be quite different was it not for the processes that control mixed layer behavior at higher latitudes. It has not escaped our attention that changes in these processes, including those that may be forced by the type of sun–earth orbital geometry changes discussed in seminal work by Milankovic (1920) and others, could provide important drivers of climate change. Further speculation on the nature and effects of such processes would be premature at this point, but may provide fertile ground for future studies.

Acknowledgments. This manuscript benefited from the constructive comments from M. Alexander and two anonymous reviewers. This publication is (partially) funded by the Joint Institute for the Study of the Atmosphere and Ocean (JISAO) under NOAA Cooperative Agreement NA17RJ1232.

APPENDIX

Sensitivity of Results to Model Parameterization

The effects of various adjustments to the model systems discussed above are summarized in Table A1. Results show that all of the adjustments considered cause changes in model behavior that are small relative to the model bias with respect to observational results.

TABLE A1. Model sensitivity to parameter adjustment. Here, $\overline{\Delta}$ is the 50°–15°S averaged difference (regular minus adjusted case) between zonally averaged results from the basic model runs (discussed in section 5) and from the run with listed adjustment; σ_Δ is the standard deviation between these two model results. The same land/near-land mask (see section 2) is used in each case. Units: °C. The last row lists values for the difference between observations and the runs discussed in section 5. Here, positive $\overline{\Delta}$ indicates an average overprediction on the part of the model; an adjustment that causes the model to fit observations perfectly would have an equal $\overline{\Delta}$ (and σ_Δ) value.

Model adjustment	KPP $\overline{\Delta}$	KPP σ_Δ	PWP $\overline{\Delta}$	PWP σ_Δ
WOA05 July initial conditions	0.08	0.03	0.07	0.02
Horizontal heat flux convergence from SODA	0.05	0.04	−0.18	0.08
$\kappa = 1 \times 10^{-4}$ m^2 s^{-1}	0.12	0.11	0.06	0.15
$\kappa = 1 \times 10^{-5}$ m^2 s^{-1}	0.06	0.03	—	—
$\kappa = 1 \times 10^{-6}$ m^2 s^{-1}	—	—	−0.09	0.05
KPP nonlocal flux term included	−0.04	0.02	N/A	N/A
Double-diffusive mixing included	0.002	0.001	N/A	N/A
Daily average (1998–2003) forcing (rather than climatological)	N/A	N/A	−0.12	0.21
Full equation of state*	−0.03	0.13	−0.41	0.04
Linear equation of state*	0.02	0.18	−0.36	0.06
Flux-corrected (detrended) run; results from 40th year	0.16	0.11	<0.01 magnitude	<0.01 magnitude
Flux-corrected (detrended) run; results from first year	<0.01 magnitude	<0.01 magnitude	<0.01 magnitude	<0.01 magnitude
Difference between standard run and observations	**0.30**	**0.58**	**0.56**	**0.62**

* These runs resolved only the upper 250 m of the water column and had $E - P$ set to zero.

REFERENCES

Antonov, J. I., R. A. Locarnini, T. P. Boyer, A. V. Mishonov, and H. E. Garcia, 2006: *Salinity*. Vol. 2, *World Ocean Atlas 2005,* NOAA Atlas NESDIS 62, 182 pp.

Bitz, C. M., M. M. Holland, E. C. Hunke, and R. E. Moritz, 2005: Maintenance of the sea-ice edge. *J. Climate,* **18,** 2903–2921.

Boyer, T. P., C. Stephens, J. I. Antonov, M. E. Conkright, R. A. Locarnini, T. D. O'Brien, and H. E. Garcia, 2002: *Salinity*. Vol. 2, *World Ocean Atlas 2001,* NOAA Atlas NESDIS 50, 165 pp.

Carton, J. A., G. Chepurin, X. Cao, and B. S. Giese, 2000: A simple ocean data assimilation of the global upper ocean: 1950–95. Part I: Methodology. *J. Phys. Oceanogr.,* **30,** 294–309.

Cherniawsky, J. Y., and J. M. Oberhuber, 1996: The seasonal cycle of mixed layer temperatures in a global general circulation model. *Climate Dyn.,* **12,** 171–183.

Chiodi, A. M., and D. E. Harrison, 2006: Summertime subtropical sea surface temperature variability. *Geophys. Res. Lett.,* **33,** L08601, doi:10.1029/2005GL024524.

——, and ——, 2007: Mechanisms of summertime subtropical southern Indian Ocean sea surface temperature variability: On the importance of humidity anomalies and the meridional advection of water vapor. *J. Climate,* **20,** 4835–4853.

——, and ——, 2008: Hurricane Alley SST variability in 2005 and 2006. *J. Climate,* **21,** 4710–4722.

Davis, R. E., R. DeSzoeke, D. Halpern, and P. Niiler, 1981: Variability in the upper ocean during MILE. Part I: The heat and momentum balances. *Deep-Sea Res.,* **28A,** 1427–1452.

de Boyer Montégut, C., G. Madec, A. S. Fischer, A. Lazar, and D. Iudicone, 2004: Mixed layer depth over the global ocean: An examination of profile data and a profile-based climatology. *J. Geophys. Res.,* **109,** C12003, doi:10.1029/2004JC002378.

Defant, A., 1961: *Physical Oceanography*. Vol. 1. MacMillan, 729 pp.

Dong, S., and K. A. Kelly, 2004: Heat budget in the Gulf Stream region: The importance of heat storage and advection. *J. Phys. Oceanogr.,* **34,** 1214–1231.

——, S. T. Gille, and J. Sprintall, 2007: An assessment of the Southern Ocean mixed layer heat budget. *J. Climate,* **20,** 4425–4442.

Ganachaud, A., and C. Wunsch, 2000: Improved estimates of global ocean circulation, heat transport and mixing from hydrographic data. *Nature,* **408,** 453–457.

——, and ——, 2003: Large-scale ocean heat and freshwater transports during the World Ocean Circulation Experiment. *J. Climate,* **16,** 696–705.

Grist, J. P., and S. A. Josey, 2003: Inverse analysis of the SOC air–sea flux climatology using ocean heat transport constraints. *J. Climate,* **16,** 3274–3295.

Jerlov, N. G., 1976: *Marine Optics.* Elsevier, 231 pp.

Josey, S. A., E. C. Kent, and P. K. Taylor, 1998: *The Southhampton Oceanography Centre (SOC) Ocean-Atmosphere Heat, Momentum and Freshwater Flux Atlas*. Southampton Oceanography Centre Rep. 6, 30 pp.

Kalnay, E., and Coauthors, 1996: The NCEP/NCAR 40-Year Reanalysis Project. *Bull. Amer. Meteor. Soc.,* **77,** 437–471.

Kara, A. B., P. A. Rochford, and H. E. Hurlburt, 2000: An optimal definition for ocean mixed layer depth. *J. Geophys. Res.,* **105,** 16 803–16 821.

——, A. J. Wallcraft, and H. E. Hurlburt, 2003: Climatological SST and MLD predictions from a global layered ocean model with an embedded mixed layer. *J. Atmos. Oceanic Technol.,* **20,** 1616–1632.

——, ——, and ——, 2007: A correction for land contamination of atmospheric variables near land–sea boundaries. *J. Phys. Oceanogr.,* **37,** 803–818.

Kimball, H. H., 1928: Amount of solar radiation that reaches the surface of the earth on the land and on the sea, and methods by which it is measured. *Mon. Wea. Rev.,* **56,** 393–398.

Large, W. G., J. C. McWilliams, and S. C. Doney, 1994: Oceanic vertical mixing: A review and a model with nonlocal boundary layer parameterization. *Rev. Geophys.,* **32,** 363–403.

Leon, S. J., 1994: *Linear Algebra with Applications*. 4th ed. MacMillan, 506 pp.

Levitus, S., 1987: A comparison of the annual cycle of two sea surface temperature climatologies of the World Ocean. *J. Phys. Oceanogr.,* **17,** 197–214.

Locarnini, R. A., A. V. Mishonov, J. I. Antonov, T. P. Boyer, and H. E. Garcia, 2006: *Temperature*. Vol. 1, *World Ocean Atlas 2005,* NOAA Atlas NESDIS 61, 182 pp.

Lorbacher, K., D. Dommenget, P. P. Niiler, and A. Köhl, 2006: Ocean mixed layer depth: A subsurface proxy for ocean-atmosphere variability. *J. Geophys. Res.,* **111,** C07010, doi:10.1029/2003JC002157.

MacCready, P., and P. Quay, 2001: Biological export flux in the Southern Ocean estimated from a climatological nitrate budget. *Deep-Sea Res. II,* **49,** 4299–4322.

Meehl, G. A., and Coauthors, 2007: Global climate projections. *Climate Change 2007: The Physical Science Basis,* S. Solomon et al., Eds., Cambridge University Press, 749–844.

Milankovic, M., 1920: *Théorie Mathématique des Phénomènes Thermiques produits par la Radiation Solaire*. Gauthier-Villars, 338 pp.

Monterey, G. I., and S. Levitus, 1997: *Climatological Cycle of Mixed Layer Depth in the World Ocean*. NOAA Atlas NESDIS 14, 5 pp. + 87 figures.

Pickard, G. L., and W. J. Emery, 1990: *Descriptive Physical Oceanography*. 5th ed. Pergamon Press, 320 pp.

Price, J. F., R. A. Weller, and R. Pinkel, 1986: Diurnal cycling: Observations on models of the upper ocean response to diurnal heating, cooling and wind mixing. *J. Geophys. Res.,* **91** (C7), 8411–8427.

Reynolds, R. W., N. A. Rayner, T. M. Smith, D. C. Stokes, and W. Wang, 2002: An improved in situ and satellite SST analysis for climate. *J. Climate,* **15,** 1609–1625.

Rintoul, S. R., and M. H. England, 2002: Ekman transport dominates air-sea fluxes in driving variability of Subantarctic Mode Water. *J. Phys. Oceanogr.,* **32,** 1308–1321.

Sallee, J. B., N. Wienders, K. Speer, and R. Morrow, 2006: Formation of subantarctic mode water in the southeastern Indian Ocean. *Ocean Dyn.,* **56,** 525–542.

Smith, S. D., 1988: Coefficients for sea surface wind stress, heat flux and wind profiles as a function of wind speed and temperature. *J. Geophys. Res.,* **93,** 15 467–15 472.

Stephens, C., J. I. Antonov, T. P. Boyer, M. E. Conkright, R. A. Locarnini, T. D. O'Brien, and H. E. Garcia, 2002: *Temperature*. Vol. 1, *World Ocean Atlas 2001,* NOAA Atlas NESDIS 49, 167 pp.

Sverdrup, H. U., M. W. Johnson, and R. H. Fleming, 1942: *The Oceans: Their Physics, Chemistry, and General Biology*. Prentice-Hall, 1087 pp.

Uppala, S. M., and Coauthors, 2005: The ERA-40 Re-Analysis. *Quart. J. Roy. Meteor. Soc.,* **131,** 2961–3012.

Woodruff, S. D., S. J. Lubker, K. Wolter, S. J. Worley, and J. D. Elms, 1993: A comprehensive ocean-atmosphere data set (COADS) release 1a: 1980–1992. *Earth Syst. Monitor,* **4,** 1–8.

Xie, P., and P. A. Arkin, 1997: Global precipitation: A 17-year monthly analysis based on gauge observations, satellite estimates, and numerical model outputs. *Bull. Amer. Meteor. Soc.,* **78,** 2539–2558.

Yu, L., and R. A. Weller, 2007: Objectively Analyzed Air-Sea heat Fluxes (OAFlux) for the global oceans. *Bull. Amer. Meteor. Soc.,* **88,** 527–539.